Optical manipulation of a multilevel nuclear spin in ZnO: Master equation and experiment

J. H. Buß,[1] J. Rudolph,[1] T. A. Wassner,[2] M. Eickhoff,[3] and D. Hägele[1]

[1]*Arbeitsgruppe Spektroskopie der kondensierten Materie, Ruhr-Universität Bochum, Universitätsstraße 150, D-44780 Bochum, Germany*

[2]*Walter Schottky Institut, Technische Universität München, Am Coulombwall 3, 85748 Garching, Germany*

[3]*Justus-Liebig-Universität Gießen, I. Physikalisches Institut, Heinrich-Buff-Ring 16, D-35392 Gießen, Germany*

(Received 12 January 2016; published 11 April 2016)

We demonstrate the dynamics and optical control of a large quantum mechanical solid state spin system consisting of a donor electron spin strongly coupled to the 9/2 nuclear spin of ^{115}In in the semiconductor ZnO. Comparison of electron spin dynamics observed by time-resolved pump-probe spectroscopy with density matrix theory reveals nuclear spin pumping via optically oriented electron spins, coherent spin-spin interaction, and quantization effects of the ten nuclear spin levels. Modulation of the optical electron spin orientation at frequencies above 1 MHz gives evidence for fast optical manipulation of the nuclear spin state.

DOI: 10.1103/PhysRevB.93.155204

I. INTRODUCTION

The control of nuclear spins in solids is an extremely attractive goal since nuclear coherence times can be six orders of magnitudes longer than lifetimes of electron spins. Applications such as a quantum spin memory or extremely sensitive magnetometry are envisioned [1]. Ensembles of nuclear spins and even single spins have been studied using nuclear magnetic resonance (NMR), electron-nuclear double resonance (ENDOR), and combinations of these methods with optical detection schemes [2,3]. Pumping of nuclear spin ensembles with optically oriented electron spins via hyperfine interaction has been used in gases since the early 1960s to dramatically increase the sensitivity of NMR [4]. In semiconductors, optical pumping schemes have since then led to the discovery and investigation of all-optical NMR, nuclear spin diffusion, focusing of precession frequencies of electron spins with different g factors, and many other effects [5–8]. The theoretical treatment of many nuclear spins coupled to an electron spin on the other side is notoriously difficult. Semiclassical methods and semianalytical solutions have been developed by several groups to deal with this so-called central spin problem [9–11].

Here we investigate a system whose coupled electron-nuclear spin dynamics is completely dominated by a single indium $I = 9/2$ nuclear spin that is strongly coupled to a single electron spin, with indium acting as a donor in the semiconductor ZnO. Such a pairwise interaction is in stark contrast to a localized electron spin in GaAs that is coupled to tens of thousands of nuclear spins with coupling constants being all on the same order [12]. Spin pairs with the nuclear partner having a large angular momentum are highly attractive for studying nonclassical quantum effects of the nuclear spin such as squeezed states [13] or cat states as realized recently in an atom-based system with $l = 25$ angular momentum states [14]. In solids, the angular momentum of the ^{13}C nucleus in the spin-spin system at an NV center in diamond or in the recently investigated SiC is with $I = 1/2$ too small to exhibit such effects [15–17]. In 2010, a first solid state based approach in bismuth-doped silicon (Si:Bi) with $I = 9/2$ was investigated by electron spin resonance (ESR) and NMR techniques and shown to be relevant for quantum information processing [18,19]. The ZnO-based system discussed here has the additional advantage of allowing for optical pumping and reading out the electron spin [3,20]. In contrast to electromagnetic fields in ESR and NMR, optical pumping can increase the coherence in the system (lower its entropy)–an important prerequisite for the increase in experimental sensitivity mentioned above and eventually for the preparation of nonclassical states. The paper presents a quantum mechanical framework for treating the electron-indium system in ZnO and shows its validity by comparison with experiment.

Figure 1 shows schematically the electron-nuclear spin system investigated here. A donor electron with its spherical s-like wave function (orange arrow on sphere indicates spin orientation) is hyperfine-coupled to the nuclear ^{115}In spin (gray arrow inside sphere). Circularly polarized laser pump pulses with modulated circular polarization (blue and red) create a paired electron (blue arrow) and hole (not shown) at the donor, a so-called D^0X exciton with a high degree of electron spin polarization along the z direction. The electron of the exciton can transfer angular momentum to the donor electron before its optical recombination within about 100 ps (determined from time-resolved photoluminescence measurements, not shown).

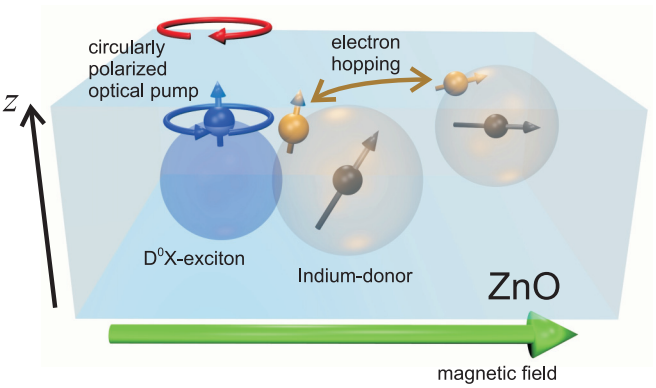

FIG. 1. The nuclear spin (gray arrow) and electron spin (orange arrow) at the ^{115}In donor form a coupled quantum mechanical system in ZnO. The spin of the donor electron is indirectly pumped via the optically excited donor-bound exciton (D^0X). Thermally activated hopping of the electron destroys entanglement between electron spin and nuclear spin.

Thermally activated electron hopping between donor sites (orange arrow) destroys spin-entanglement within the coupled spin system.

In the following, we will first theoretically treat this system by a master equation for the full two-spin density matrix before comparing the simulations to experimental results obtained from time-resolved Kerr-rotation (TRKR) spectroscopy where the electron spin dynamics is monitored by optical probe pulses. Going beyond earlier theoretical approaches [21,22], we will not only include electron spin relaxation in the theory but also optical pumping and electron hopping among donor sites.

II. MASTER EQUATION OF SPIN DYNAMICS

The dynamics of the interacting electron spin $\vec{s}$ and the nuclear spin $\vec{I}$ in a magnetic field $\vec{B}$ is given by the Hamiltonian [3]

$$H = \beta g^{(e)} \vec{B} \cdot \vec{s} + A\vec{I} \cdot \vec{s} + P_{\parallel} I_z^2 - \beta g^{(n)} \vec{B} \cdot \vec{I}, \qquad (1)$$

where the first and last term describe the electronic and nuclear spin precession in the external magnetic field $\vec{B}$. The hyperfine coupling is described by the second term. The third term is due to a weak electric quadrupole crystal field splitting that in principle can be exploited for spin squeezing [13]. The following parameters are known from ENDOR experiments (see Ref. [3]): $\beta g^{(e)}/h = 0.172\,\mathrm{THz\,T^{-1}}$ ($g^{(e)} = 1.96$), $\beta g^{(n)}/h = 9.329\,\mathrm{MHz\,T^{-1}}$, $A/h = 100.2\,\mathrm{MHz}$, and $P_{\parallel}/h = 1.27$ MHz. The electron-nuclear system is fully described by a density matrix ρ in the 20-dimensional combined Hilbert space $H_n \otimes H_e$ for nuclear spin and electron spin. The master equation

$$\dot{\rho} = \frac{i}{\hbar}[\rho, H] + \Gamma_{\mathrm{relax}} + \Gamma_{\mathrm{hop}} \qquad (2)$$

describes both the coherent propagation (first term) and dissipative coupling to the environment (last two terms). The relaxation of the electron spin towards its equilibrium orientation $\rho_{\mathrm{final}} \propto \exp(-\beta g^{(e)} \vec{B}\vec{s}/k_B T)$ is in the most simple form of isotropic relaxation given by (see Appendix A)

$$\Gamma_{\mathrm{relax}} = -\gamma_{\mathrm{relax}}[\rho - (\mathrm{Tr}_e \rho) \otimes \rho_{\mathrm{final}}], \qquad (3)$$

with the spin relaxation rate γ_{relax}. The symbol Tr_e denotes the partial trace over the density matrix with respect to the electronic subsystem. The nuclear state $\mathrm{Tr}_e \rho$ may be interpreted as a spin state that has lost all entanglement with the electronic state. In addition to spin relaxation, we also regard the effect of a thermally activated electron exchanging its site with some random neighboring donor electron (hopping). While in this case the nuclear and electronic spin states will be largely conserved, the entanglement between both is lost. Consequently, the initial state will relax with the hopping rate γ_{hop} towards such a state:

$$\Gamma_{\mathrm{hop}} = -\gamma_{\mathrm{hop}}[\rho - (\mathrm{Tr}_e \rho) \otimes (\mathrm{Tr}_n \rho)]. \qquad (4)$$

A repetitive laser excitation creates partially spin polarized electrons ρ_{L} that exchange spin with the donor-bound electrons giving rise to a new spin-spin density matrix ρ' after each excitation pulse

$$\rho' = p(\mathrm{Tr}_e \rho) \otimes \rho_{\mathrm{L}} + (1-p)\rho. \qquad (5)$$

A parameter value $p = 0.5$ corresponds to a balanced mixing between the donor-bound electron spin and the laser-generated spin. We are aware that an analytical treatment of the Hamiltonian is possible for $P_{\parallel} = 0$ or $\vec{B}$ along the z direction [21], but decided to restrain ourselves to a numerical treatment which allows for the treatment of $P_{\parallel} \neq 0$, inclusion of damping mechanisms, and arbitrary magnetic field orientations.

The density matrix $\rho(t)$ is obtained by numerically integrating the equation of motion for a time span of 200 laser pulses with a fully random spin distribution $\rho = \frac{1}{20}\mathbb{1}$ as initial condition. Laser excitation and electron spin relaxation drive the system into a dynamics $\rho(t)$ which we find to be independent from the initial state after less than 100 pulses. The temporal traces are then obtained from averaging the z-spin orientation $S_z(t) = \mathrm{Tr}[\sigma_z \rho(t)]$ for the subsequent 100 temporal intervals of length τ_{rep}, where σ_z is the Pauli spin matrix for the z direction. We fix the spin relaxation rate to $\gamma_{\mathrm{relax}} = 1/(20\,\mathrm{ns})$ which is close to reported values [20] and use a hopping rate $\gamma_{\mathrm{hop}} = 1/(4\,\mathrm{ns})$. The induced electron spin state ρ_{L} after absorption of a laser pulse is given by the 2×2 matrix $\rho_{\mathrm{L}} = \frac{1}{2}\mathbb{1} + \alpha_{\mathrm{L}} s_z$ where α_{L} is the degree of spin polarization. The value $\alpha_{\mathrm{L}} = 0.3$ takes into account optical selection rules and spin relaxation via exchange coupling with optically created holes which rapidly decreases the spin polarization during the exciton lifetime [23]. The mixing parameter is assumed to be $p = 0.5$, estimated from the excitation density in comparison with the donor density. In the case of laser polarization modulated with frequency f_{m}, the polarization of a laser pulse at time t_j is given by $\alpha_{\mathrm{L}} = \alpha \sin[\frac{1}{2}\cos(2\pi f_{\mathrm{m}} t_j)]$ with $\alpha = 0.3$. The actual value of $P_{\parallel}$ can vary slightly in different samples due to strain [24]. The calculated electron spin transients show, however, no visible dependence on $P_{\parallel}$ as the dipolar hyperfine coupling completely dominates the dynamics.

III. SIMULATIONS

Figure 2 shows the calculated electron spin dynamics for pulsed optical excitation with fixed circular polarization and a repetition interval of $\tau_{\mathrm{rep}} = 12.5$ ns between consecutive laser pulses. The dynamics falls into two regimes with different characteristics:

(i) In the regime of high in-plane magnetic fields $B >$ 25 mT, the electron spin shows rapid spin precession with an additional beating pattern of the amplitude. A pronounced maximum in the beating pattern appears 10 ns after excitation. This can be explained by considering the eigenstates

$$|m_s; m_I\rangle \qquad (6)$$

with $m_I = -9/2, -7/2, \ldots, 9/2$ for the nuclear spin and $m_s = -1/2, 1/2$ for the electron spin with eigenenergies

$$E_{m_I, m_s} = (\beta g^{(n)} B_z + m_s A) m_I. \qquad (7)$$

The eigenenergies give rise to ten different precession frequencies of the electron spin with $\hbar\omega_{m_I} = E_{m_I,1/2} - E_{m_I,-1/2}$ that depend linearly on m_I. Destructive interference of all ten oscillations leads to 9 nodes in the amplitude of the electron precession with a temporal distance of $h/(10A) \approx 1$ ns.

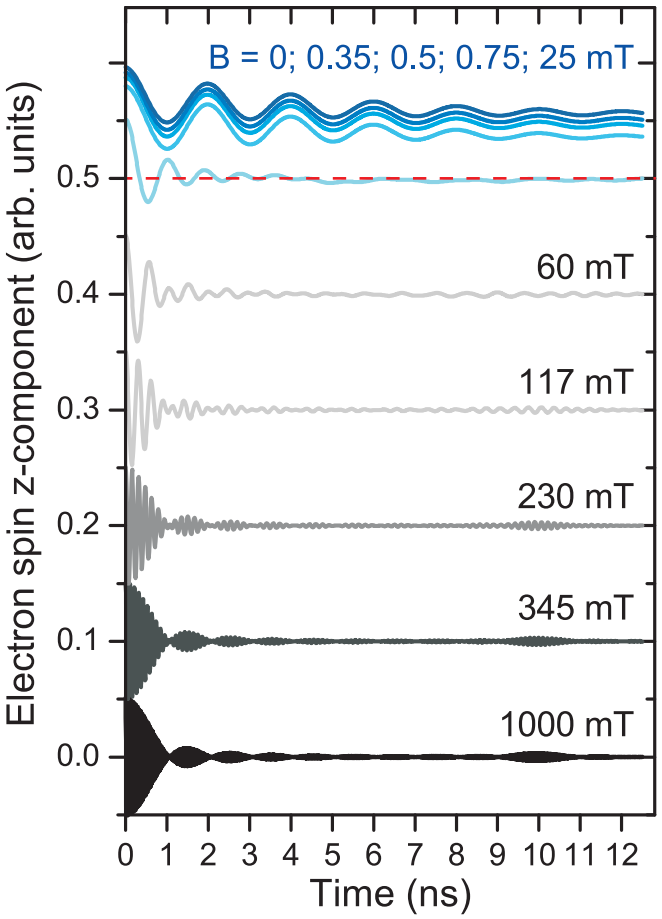

FIG. 2. Calculated spin dynamics of an electron coupled to a 9/2 indium nuclear spin in ZnO after pulsed optical excitation for different magnetic fields. Curves are offset for clarity. An identical offset of 0.5 was used for all transients below with $B < 60$ mT (blue curves).

Constructive interference leads after a time $h/A \approx 10$ ns to a pronounced rephasing effect [20,22].

(ii) In the opposite regime of vanishing external magnetic fields, the electron spin dynamics corresponds to two spins precessing around each other, resulting in a single oscillation frequency. In this case, the spin dynamics is governed by the term $\vec{I} \cdot \vec{s}$ in the Hamiltonian which possesses only two different eigenvalues: $-\frac{1}{2}(I+1)$ and $\frac{1}{2}I$ (see Ref. [25] and Appendix B). Beating between these states consequently gives rise to a single nonzero beating energy of $(I+\frac{1}{2})A$ matching exactly the precession period of 2 ns seen in the simulations.

The electron spin transient shows a large offset at magnetic fields close to zero. The offset originates from the polarization of the indium nuclear spin along the z direction. The hyperfine field of the nuclear spin stabilizes the electron spin in the z direction resulting in the observed offset. Oscillations in the hyperfine field are, however, always observed as even the maximally aligned $I_z = 9/2$ nuclear spin state shows quantum mechanical uncertainty in the x and y direction which induces electron spin precession. The nuclear polarization is a known consequence of repetitive pumping of the electron spin with fixed polarization ($f_m = 0$) which leads to the transfer of angular momentum from the electron spin to the nuclear spin

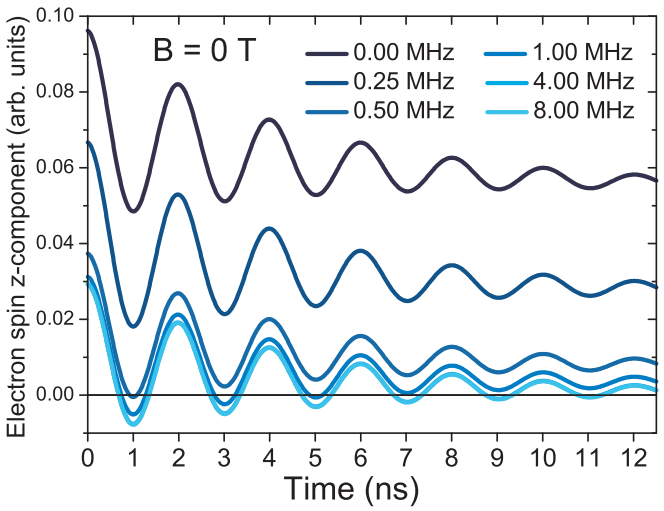

FIG. 3. Calculated time-dependent electron spin orientation for increasing pump polarization modulation frequencies f_m. The transition from nuclear spin orientation to spin randomization causes a decreasing offset of the oscillating transient.

(so-called dynamical nuclear polarization) [6]. The nuclear polarization can be suppressed via fast modulation of the optically pumped electron spin orientation which leads to a reduction of the offset: Figure 3 shows transients for optical excitation modulated between σ^+ and σ^- circular polarization at zero magnetic field. In the case of large modulation frequencies f_m beyond about 1 MHz, the slow dynamics of the nuclear spin, together with an electron spin polarization being zero on average, leads to a complete randomization of the nuclear spin. Nuclear spins oriented perpendicular to z will then cause an electron spin precession with oscillations between $s_z = 1/2$ and nearly $s_z = -1/2$. This leads to an overall average dynamics with a much smaller polarization offset compared to the unmodulated case. The offset level is reduced to about 50% at $f_m = 0.25$ MHz showing that the nuclear spin is no longer able to fully follow a modulated electron spin orientation within a time span of about 2 μs corresponding to 160 laser pulses. This appears to be a sensible number as at least five subsequently created electrons would be required to flip their spin fully and transfer angular momentum to the nuclear spin to obtain a reversal of the nuclear spin from 9/2 to $-9/2$. However, the electron spin flips will never be complete as the spin is stabilized by the z-oriented nuclear spin. We are aware that in the limit of short coherence times between electron spin and nuclear spin and near thermal equilibrium the reorientation time would be basically given by the nuclear T_1 time (see Chap. IX.C in Ref. [26]). In our case of long coherence times a similarly simple relation is not known to us. We therefore rely here on the full numerics to obtain the offset in dependence on frequency. While a better qualitative understanding is certainly desirable in the future, we will show below that our calculations quantitatively agree very well with experiment. We note that the recently observed reduction of spin polarization in flourine-doped ZnSe with increasing modulation frequency was caused by a different effect independent from hyperfine fields. A very long electron spin lifetime in ZnSe which is longer than the modulation

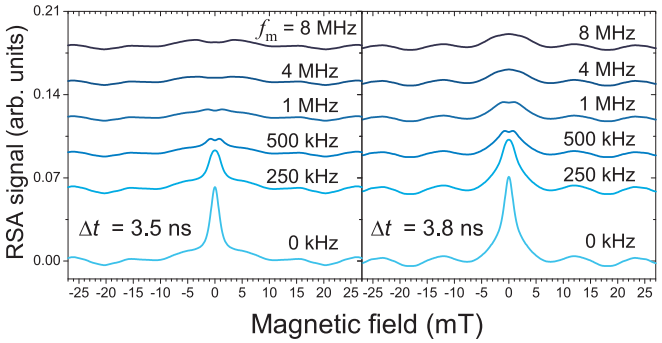

FIG. 4. Calculated signal of RSA 3.5 ns and 3.8 ns after the laser pump pulse for increasing polarization modulation frequencies f_m. The disappearance of the central peak follows the reduction of the nuclear polarization in the z direction.

interval $\gamma_s^{-1} \gg f_m^{-1}$ leads effectively to a temporal average of the laser pulse polarization causing a reduction of the electron spin polarization [27]. The large offset in our case relies on a strong hyperfine field. A reduction of spin polarization is found already for slow modulation with $f_m < \gamma_{relax}$ which is opposite to the ZnSe case.

In the following we discuss calculations of the magnetic-field-dependent TRKR signal at fixed temporal delays Δt (Fig. 4). These so-called resonant spin amplification (RSA) curves were experimentally pioneered by Kikkawa *et al.* [28] and have been used by many groups for studying systems with long spin lifetimes or an anisotropic spin relaxation tensor [29]. We find a strong central peak for low modulation frequencies f_m of the pump pulse polarization that disappears for high modulation frequencies, which is a clear signature of nuclear spin pumping and randomization as discussed before (Fig. 3). The oscillatory behavior for increasing fields is a signature of the increasing spin precession angle. Strong central peaks were also observed in the case of anisotropic spin relaxation in, e.g., (110) GaAs quantum wells where the z-spin relaxation is very weak [29]. The intrinsic electron spin relaxation in our model is, however, fully isotropic and the central peak is solely a consequence of nuclear spin pumping and hyperfine interaction.

Concluding the theoretical part, we emphasize that the features of rephasing and nuclear spin pumping can be obtained from theory also when the hopping term Γ_{hop} is neglected. We decided to keep the term as for higher temperatures (not discussed in this paper) a large γ_{hop} will be able to describe a complete vanishing of the rephasing effect together with even increased spin lifetimes due to motional narrowing while this is not possible with a single parameter γ_{relax}. In the present case of low temperatures the choice for γ_{hop} and γ_{relax} has to regard that both reduce the rephasing amplitude but only γ_{relax} reduces the nuclear spin pumping effect–which explains our choice of the parameters.

IV. SAMPLE AND EXPERIMENT

Finally, we compare the predictions from above with data from TRKR on ZnO. The investigated ZnO sample was grown by plasma-assisted molecular beam epitaxy according to the growth procedure described in Ref. [30]. A 250-nm-thick ZnO layer was grown at a substrate temperature of 500 °C on a MgO/ZnO double buffer layer on a (0001) sapphire substrate. Unintentional doping with In and Al impurities leads to an n-type carrier density of about $n_D = 1\times10^{18}$ cm^{-3}. The ZnO layer was capped with 50 nm $ZnMg_{0.19}O_{0.81}$ to suppress surface effects [31]. The sample was mounted in a cold-finger cryostat allowing for temperatures down to $T = 10$ K. An external magnetic field B up to 1 T was applied in the sample plane. For measurements in zero magnetic field, the cryostat was shielded by an additional mu-metal shield to suppress residual static magnetic fields.

TRKR was measured with the setup described in Ref. [32]. Laser pulses were additionally shaped by a grating pulse shaper to a spectral width of approximately 5.5 meV centered at 3.356 eV to resonantly excite the In-donor-bound exciton. The pump beam polarization was modulated between right and left circularly polarized by an electro-optic modulator at a modulation frequency f_m between 50 kHz and 8 MHz. The average pump and probe power was 10 mW and 1 mW, respectively, corresponding to a density of photoexcited carriers of approximately 10^{17} cm^{-3}.

Figure 5 shows TRKR measurements for increasing magnetic fields between 0 and 1 T. All data were taken at a sample

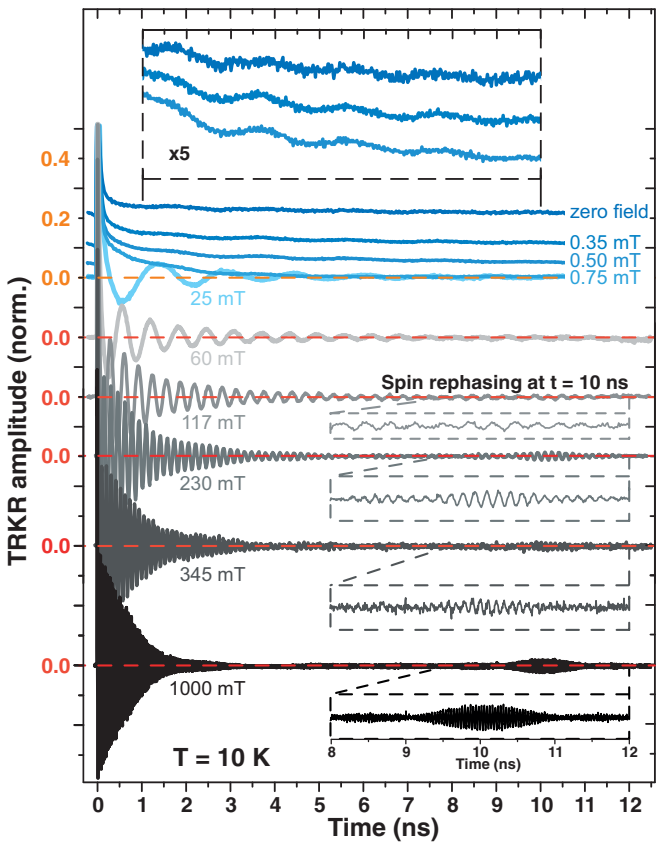

FIG. 5. Measured transients of the electron spin signal in z direction for different magnetic fields at $T = 10$ K (compare theoretical curves in Fig. 2). The signal originates from a superposition of electron spin dynamics at the indium donor and an exponentially decaying signal from electrons at the aluminum donors. The blue curves share the same offset. The inset shows vertically shifted magnified transients for the three lowest fields showing a 2 ns periodic behavior as predicted.

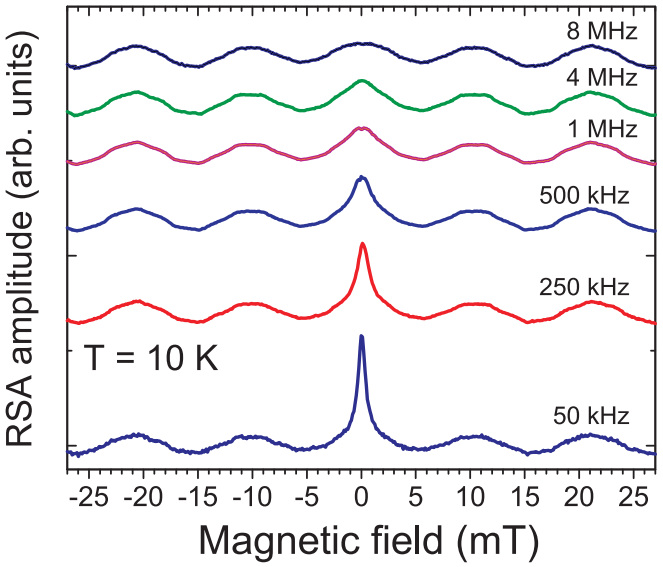

FIG. 6. Measured resonant spin amplification for increasing pump polarization modulation frequencies f_m at $T = 10$ K (compare Fig. 4). The height of the central peak reveals frequency-dependent nuclear spin pumping.

temperature of 10 K. The rephasing effect at $t = 10$ ns is clearly visible for fields above 100 mT (compare Fig. 2). The amplitude of the oscillations in the interval between 8 to 12 ns after laser excitation shows also good agreement with the calculated behavior. At early times a much less pronounced beating pattern is observed caused by a superimposed signal from electrons residing at additional aluminum donors present in the sample [20]. These electrons are subject to a much weaker nuclear field and exhibit therefore the precessional behavior of a free electron in an external magnetic field [33]. At later times the signal from the electrons at the aluminum donor has almost disappeared. The precession of the electron spin with a period of 2 ns in the hyperfine field is clearly visible for magnetic fields below 1 mT (see inset). The decrease of the positive offset is, however, much stronger in the experimental data as the spins of the electrons at Al donors start precessing in the external field which leads to a strong reduction of the offset.

The strong influence of nuclear spin pumping on the dynamics of the electron spin is demonstrated by the experimental RSA scans at $\Delta t = 3.5$ ns shown in Fig. 6 for varying modulation frequencies. The strong central peak which is due to the nuclear spin stabilizing the electron spin in the excitation direction decreases with increasing frequency as predicted by our calculations shown in Fig. 4. The oscillations around the central peak are mainly due to signal from the Al-donor electron and do not exactly match the corresponding calculation for a time delay $\Delta t = 3.5$ ns. A better agreement is found for $\Delta t = 3.8$ ns when the calculated dynamics coincidentally matches that of the common signal from the Al and In donor. Lee *et al.* also discovered a strong central peak in their RSA experiments on ZnO but ascribed it to a strongly anisotropic electron spin relaxation mechanism with long spin lifetimes for z-oriented spins [34]. Our own experiments, however, exhibit a decrease of the central peak with increasing f_m in agreement with nuclear spin pumping and in contradiction to Lee's relaxation mechanism that should not depend on f_m. We note that a recent theory of spin relaxation in ZnO also disregards nuclear effects [35].

In conclusion, we demonstrated the control and readout of a large solid state quantum system via optical laser spectroscopy. The TRKR and RSA experiments are extremely well described by density matrix theory including optical electron spin orientation, spin relaxation, and hopping mechanisms. This opens a way for investigating approaches for creating nonclassical nuclear quantum states in the ZnO or similar system. The theoretical treatment of finite-temperature effects (hopping) and imperfect optical spin selection rules will allow for a realistic assessment of such systems. In the future, an interplay of multipulse optical pumping and the inherent non-nonlinear I_z^2 part of the Hamiltonian are envisioned to eventually create nonclassical angular momentum quantum states of the 9/2 indium nuclear spin.

ACKNOWLEDGMENT

We gratefully acknowledge financial support by the German Science Foundation (DFG priority program 1285 Semiconductor Spintronics).

APPENDIX A: MASTER EQUATION APPROACH TO ELECTRON SPIN RELAXATION

In the following we show that Eq. (3)

$$\Gamma_{\text{relax}} = -\gamma_{\text{relax}}[\rho - (\text{Tr}_e\rho) \otimes \rho_{\text{final}}] \tag{A1}$$

correctly describes isotropic spin relaxation towards the equilibrium spin state ρ_{final}. The derivation follows the standard quantum mechanical theory of damping [36]. The usual equation of motion of a quantum mechanical system

$$\dot{\rho} = \frac{i}{\hbar}[\rho, H] \tag{A2}$$

describes its coherent evolution but does not include damping. Therefore, damping needs to be included by coupling the system ρ to an external reservoir (bath) ρ^{b}. In the context of spin relaxation of conduction band electrons, spin orbit coupling of the electron spin to a bath of orbital degrees of freedom leads to the celebrated Dyakonov-Perel (DP) spin relaxation [37]. The relaxation term of Dyakonov and Perel, however, always leads to a fully randomized spin orientation which is not correct for spins in finite magnetic fields. Therefore, we chose instead of the orbital degree of freedom another spin 1/2 particle that is supposed to be in the relaxed state ρ^{b} and interacts for a short time with the donor spin system. Relaxation towards the correct final state will be recovered as shown below. The temporary interaction is modeled by a gate function $g(t)$. The Hamiltonian of the full system

$$\tilde{H}(t) = H + \lambda g(t) \underbrace{\sum_{i,j=x,y,z} C_{i,j} s_i s_j^{\text{b}}}_{V_{\text{spin}}} \tag{A3}$$

now propagates the combined initial density matrix $\tilde{\rho}_0 = \rho \otimes \rho^{\text{b}}$ of system and bath. The tensor $C_{i,j}$ describes the spin-spin interaction in a general form that in principle allows for the

description of anisotropic spin relaxation. After the interaction, the system's density matrix ρ is recovered from $\tilde{\rho}$ by taking the trace $\rho = \mathrm{Tr}_\mathrm{b}\tilde{\rho}$ over the reservoir [see Eq. (A7)]. The dynamics is calculated by using the method of successive approximation. With the ansatz $\tilde{\rho}(t) = \tilde{\rho}_0 + \lambda\tilde{\rho}_1(t) + \lambda^2\tilde{\rho}_2(t)$ and the Schrödinger equation $\dot{\tilde{\rho}}(t) = \frac{i}{\hbar}[\tilde{\rho}(t), \tilde{H}(t)]$ we obtain by comparison of orders in λ and formal integration the solution

$$\tilde{\rho}_1(t) = \frac{i}{\hbar}G(t)[\tilde{\rho}_0, V_\mathrm{spin}], \tag{A4}$$

$$\tilde{\rho}_2(t) = -\frac{G(t)^2}{2\hbar^2}[[\tilde{\rho}_0, V_\mathrm{spin}], V_\mathrm{spin}], \tag{A5}$$

where $G(t) = \int_{-\infty}^{t} g(t')\,dt'$ is the integral of the gate function, with $G(-\infty) = 0$ and G getting constant after interaction. Here we neglected H as we assume a much faster dynamics induced by V_spin compared with the slow dynamics driven by H. The double commutator in Eq. (A5) is found in all damping theories based on the master equation [36–38]. This first term depends on the overall sign of $C_{i,j}$ while the second-order term is independent. Assuming a second bath with an interaction tensor $-C_{i,j}$ would give the same second-order relaxation term but at the same time cancel the first-order term. We will therefore neglect the first-order term (A4).

The density matrix $\tilde{\rho}_0$ is an element of a Hilbert space that is a direct product of the Hilbert spaces of the nuclear spin, the donor electron spin, and the bath spin. A matrix element $(\tilde{\rho}_0)_{\mu,i,j;\mu',i',j'}$ therefore exhibits indices of all three subspaces. In the following we use matrix notation for the donor electron spin and bath spin subspace and index notation (μ,μ' indices) for the nuclear spin subspace. We now can calculate the double commutator for

$$(\tilde{\rho}_0)_{\mu,\mu'} = a_{\mu,\mu'}\begin{pmatrix}\rho_{11}(\mu,\mu') & \rho_{12}(\mu,\mu')\\ \rho_{21}(\mu,\mu') & \rho_{22}(\mu,\mu')\end{pmatrix}\otimes\begin{pmatrix}\rho^\mathrm{b}_{11} & \rho^\mathrm{b}_{12}\\ \rho^\mathrm{b}_{21} & \rho^\mathrm{b}_{22}\end{pmatrix} \tag{A6}$$

and find for isotropic spin-spin interaction with $C_{i,j} = \pm\epsilon$ for $i = j$ and $C_{i,j} = 0$ otherwise the second-order term with the help of an algebra system

$$\mathrm{Tr}_\mathrm{b}[\rho_2(t)]_{\mu,\mu'} = \frac{a_{\mu,\mu'}\epsilon^2 G(t)}{4\hbar^2}\begin{pmatrix}\rho_{22}\rho^\mathrm{b}_{11} - \rho_{11}\rho^\mathrm{b}_{22} & -\rho_{12}\left(\rho^\mathrm{b}_{11} + \rho^\mathrm{b}_{22}\right) + \rho^\mathrm{b}_{12}(\rho_{11} + \rho_{22})\\ -\rho_{21}\left(\rho^\mathrm{b}_{11} + \rho^\mathrm{b}_{22}\right) + \rho^\mathrm{b}_{21}(\rho_{11} + \rho_{22}) & -\rho_{22}\rho^\mathrm{b}_{11} + \rho_{11}\rho^\mathrm{b}_{22}\end{pmatrix}, \tag{A7}$$

where we suppressed the notation of the (μ,μ') dependence of $\rho_{i,i'}$ on the right-hand side.

The right-hand side simplifies with $\rho_{11} + \rho_{22} = 1$ and $\rho^\mathrm{b}_{11} + \rho^\mathrm{b}_{22} = 1$ to

$$\mathrm{Tr}_\mathrm{b}[\tilde{\rho}_2(t)]_{\mu,\mu'} = \frac{a_{\mu,\mu'}\epsilon^2 G(t)^2}{4\hbar^2}\begin{pmatrix}-\left(\rho_{11} - \rho^\mathrm{b}_{11}\right) & -\left(\rho_{12} - \rho^\mathrm{b}_{12}\right)\\ -\left(\rho_{21} - \rho^\mathrm{b}_{21}\right) & -\left(\rho_{22} - \rho^\mathrm{b}_{22}\right)\end{pmatrix} \tag{A8}$$

$$= -\frac{a_{\mu,\mu'}\epsilon^2 G(t)^2}{4\hbar^2}\left(\rho^\mathrm{e}_{\mu,\mu'} - \rho_\mathrm{final}\right), \tag{A9}$$

where ρ_final is a state of the donor electron that is identical to the spin state of the bath. Using pure matrix notation the last line becomes

$$\mathrm{Tr}_\mathrm{b}[\tilde{\rho}_2(t)] = -\frac{\epsilon^2 G(t)^2}{4\hbar^2}[\rho - (\mathrm{Tr}_e\rho)\otimes\rho_\mathrm{final}], \tag{A10}$$

where we used the property $(\mathrm{Tr}_\mathrm{e}\rho)_{\mu,\mu'} = a_{\mu,\mu'}$ with Tr_e being the partial trace over the electron spin degrees of freedom. Assuming a steady supply of external thermal spins with rate γ_bath we are able to incorporate the effect of the external spins ρ^b into the master equation for the system. The scattering contribution is eventually given by a term of the form

$$\begin{aligned}\Gamma_\mathrm{relax} &= \gamma_\mathrm{bath}\mathrm{Tr}_\mathrm{b}[\tilde{\rho}_2(\infty)]\\ &= -\gamma_\mathrm{relax}[\rho - (\mathrm{Tr}_e\rho)\otimes\rho_\mathrm{final}],\end{aligned} \tag{A11}$$

as used in our paper.

APPENDIX B: THE EIGENVALUES OF $\vec{I}\cdot\vec{s}$

The most direct way of showing that $\frac{1}{2}I$ and $-\frac{1}{2}(I+1)$ are the only eigenvalues of $\vec{I}\cdot\vec{s}$ is to show that the polynomial $p(x) = (x - \frac{1}{2}I)[x + \frac{1}{2}(I+1)]$ is zero for $x = \vec{I}\cdot\vec{s}$ (Cayley-Hamilton theorem). We make use of the relations $s_j^2 = \mathbb{1}/4$ for $j = x,y,z$ and the relations $s_x s_y = i\frac{1}{2}s_z$ and $I_x I_y - I_y I_x = i I_z$ that hold for all cyclic permutations of x,y,z:

$$p(\vec{I}\vec{s}) = (\vec{I}\cdot\vec{s})(\vec{I}\cdot\vec{s}) + \tfrac{1}{2}\vec{I}\cdot\vec{s} - \tfrac{1}{4}I(I+1) \tag{B1}$$

$$\begin{aligned}&= \left(I_x^2 s_x^2 + I_y^2 s_y^2 + I_z^2 s_z^2\right)\\ &\quad + I_x I_y s_x s_y + I_y I_x s_y s_x + \text{cycl. perm.}\\ &\quad + \tfrac{1}{2}\vec{I}\cdot\vec{s} - \tfrac{1}{4}I(I+1)\end{aligned} \tag{B2}$$

$$\begin{aligned}&= \tfrac{1}{4}I(I+1)\\ &\quad + I_x I_y \tfrac{1}{2}i s_z - I_y I_x \tfrac{1}{2}i s_z + \text{cycl. perm.}\\ &\quad + \tfrac{1}{2}\vec{I}\cdot\vec{s} - \tfrac{1}{4}I(I+1)\end{aligned} \tag{B3}$$

$$\begin{aligned}&= -\tfrac{1}{2}I_z s_z + \text{cycl. perm.}\\ &\quad + \tfrac{1}{2}\vec{I}\cdot\vec{s}\end{aligned} \tag{B4}$$

$$= 0. \tag{B5}$$

[1] C. Boehme and D. R. McCamey, Science **336**, 1239 (2012).
[2] W. G. Breiland, C. B. Harris, and A. Pines, Phys. Rev. Lett. **30**, 158 (1973).
[3] D. Block, A. Herve, and R. T. Cox, Phys. Rev. B **25**, 6049 (1982).
[4] M. A. Bouchiat, T. R. Carver, and C. M. Varnum, Phys. Rev. Lett. **5**, 373 (1960).
[5] G. Lampel, Phys. Rev. Lett. **20**, 491 (1968).
[6] D. Paget, Phys. Rev. B **25**, 4444 (1982).
[7] J. M. Kikkawa and D. D. Awschalom, Science **287**, 473 (2000).
[8] A. Greilich, A. Shabaev, D. R. Yakovlev, A. L. Efros, I. A. Yugova, D. Reuter, A. D. Wieck, and M. Bayer, Science **317**, 1896 (2007).
[9] E. Barnes, Ł. Cywiński, and S. Das Sarma, Phys. Rev. Lett. **109**, 140403 (2012).
[10] A. Faribault and D. Schuricht, Phys. Rev. Lett. **110**, 040405 (2013).
[11] D. Stanek, C. Raas, and G. S. Uhrig, Phys. Rev. B **90**, 064301 (2014).
[12] B. Urbaszek, X. Marie, T. Amand, O. Krebs, P. Voisin, P. Maletinsky, A. Högele, and A. Imamoglu, Rev. Mod. Phys. **85**, 79 (2013).
[13] M. Kitagawa and M. Ueda, Phys. Rev. A **47**, 5138 (1993).
[14] A. Signoles, A. Facon, D. Grosso, I. Dotsenko, S. Haroche, J.-M. Raimond, M. Brune, and S. Gleyzes, Nat. Phys. **10**, 715 (2014).
[15] F. Jelezko, T. Gaebel, I. Popa, M. Domhan, A. Gruber, and J. Wrachtrup, Phys. Rev. Lett. **93**, 130501 (2004).
[16] A. L. Falk, P. V. Klimov, V. Ivady, K. Szasz, D. J. Christle, W. F. Koehl, A. Gali, and D. D. Awschalom, Phys. Rev. Lett. **114**, 247603 (2015).
[17] V. Ivady, K. Szasz, A. L. Falk, P. V. Klimov, D. J. Christle, E. Janzen, I. A. Abrikosov, D. D. Awschalom, and A. Gali, Phys. Rev. B **92**, 115206 (2015).
[18] G. W. Morley, M. Warner, A. M. Stoneham, P. T. Greenland, J. van Tol, C. W. M. Kay, and G. Aeppli, Nat. Mater. **9**, 725 (2010).
[19] G. W. Morley, P. Lueders, M. H. Mohammady, S. J. Balian, G. Aeppli, C. W. M. Kay, W. M. Witzel, G. Jeschkem, and T. S. Monteiro, Nat. Mater. **12**, 103 (2013).
[20] S. Kuhlen, Spinkohärenz und Spindynamik in Zinkoxid, Ph.D. thesis, RWTH Aachen, 2014.
[21] M. H. Mohammady, G. W. Morley, A. Nazir, and T. S. Monteiro, Phys. Rev. B **85**, 094404 (2012).
[22] S. Cronenberger, M. Vladimirova, S. V. Andreev, M. B. Lifshits, and D. Scalbert, Phys. Rev. Lett. **110**, 077403 (2013).
[23] S. Pfalz, R. Winkler, T. Nowitzki, D. Reuter, A. D. Wieck, D. Hägele, and M. Oestreich, Phys. Rev. B **71**, 165305 (2005).
[24] R. Böttcher, A. Pöppl, M. Lorenz, S. Friedländer, D. Spemann, and M. Grundmann, J. Magn. Reson. **245**, 79 (2014).
[25] H. Haken and H. C. Wolff, *The Physics of Atoms and Quanta* (Springer Verlag, Berlin, 2005).
[26] A. Abragam, *Principles of Nuclear Magnetism* (Oxford University Press, London, 1961).
[27] F. Heisterkamp, E. A. Zhukov, A. Greilich, D. R. Yakovlev, V. L. Korenev, A. Pawlis, and M. Bayer, Phys. Rev. B **91**, 235432 (2015).
[28] J. M. Kikkawa and D. D. Awschalom, Phys. Rev. Lett. **80**, 4313 (1998).
[29] M. Griesbeck, M. M. Glazov, E. Y. Sherman, D. Schuh, W. Wegscheider, C. Schüller, and T. Korn, Phys. Rev. B **85**, 085313 (2012).
[30] T. A. Wassner, B. Laumer, S. Meier, A. Laufer, B. K. Meyer, M. Stutzmann, and M. Eickhoff, J. Appl. Phys. **105**, 023505 (2009).
[31] B. Laumer, T. A. Wassner, F. Schuster, M. Stutzmann, J. Schörmann, M. Rohnke, A. Chernikov, V. Bornwasser, M. Koch, S. Chatterjee, and M. Eickhoff, J. Appl. Phys. **110**, 093513 (2011).
[32] J. H. Buß, J. Rudolph, S. Shvarkov, H. Hardtdegen, A. D. Wieck, and D. Hägele, Appl. Phys. Lett. **102**, 192102 (2013).
[33] The separated measurement of the two donor species is in principe possible using ps-laser pump and probe pulses from two synchronized lasers as demonstrated in Ref. [20].
[34] J. Lee, A. Venugopal, and V. Sih, Appl. Phys. Lett. **106**, 012403 (2015).
[35] N. J. Harmon, W. O. Putikka, and R. Joynt, Phys. Rev. B **79**, 115204 (2009).
[36] M. O. Scully and M. S. Zubairy, *Quantum Optics* (Cambridge University Press, Cambridge, 1997).
[37] M. I. Dyakonov and V. I. Perel', Fiz. Tverd. Tela **13**, 3581 (1971) [Sov. Phys. Solid State **13**, 3023 (1972)].
[38] M. Goldman, Adv. Magn. Reson. **149**, 160 (2001).